

---

# Advances in Linear Array Continuous Ink Jet Droplet Charging and Deflection

**Randy Fagerquist**

**Scitex Digital Printing, Inc., Dayton, Ohio**

---

## Introduction

The control of ink droplets in a conventional binary continuous ink jet printer is generally accomplished by charging or not charging the ink droplets as they separate from the jet. The charged droplets can be electrostatically deflected to a device for ink recirculation or to the print substrate. In our printers, the charged droplets are not printed and are directed to a catcher assembly for recirculation. The uncharged droplets are allowed to exit the print head and impact the substrate.

Successful exploitation of droplet charging and deflection mechanisms is important to optimum printer operation and reliability. We have made a substantial effort to increase the understanding of these mechanisms, and will present some of our results concerning the fundamentals of droplet charging and deflection in this paper.

The experimental results reported here were obtained using a modified planar charging print head design. A partial drawing of an unmodified print head is shown as Figure 1. The charge electrodes, catcher, and ink jets/filaments are shown for a standard planar charging print head. An additional mass charging electrode was added to the print head for this study and positioned opposite the jets from and parallel to the standard charge plate. The placement of the mass electrode was chosen so as to center the jets between the two electrode structures. Figure 2 shows an edge view of the print head along with the position of the mass electrode and the trajectory of a typical stimulated jet.

The modified print head was used in an extensive set of charging and deflection experiments. The data from these experiments were analyzed in the framework of an existing and a recently developed model for droplet deflection.

## Present Deflection Model

Katerberg<sup>1</sup> modeled the print head droplet deflection (henceforth referred to as the JK model) and identified three mechanisms that account for most, if not all, of the observed droplet deflection in the planar charging

print head. These are: 1) jet or filament bending, 2) lead deflection, and 3) image force attraction. The following is a brief summary of his model.

### Jet Bending

The droplets, just before breaking away from the conducting ink filaments, are electrostatically attracted to the charge electrode. The droplet can be considered as one "plate" of a parallel plate capacitor with the charge electrode as the opposing plate. The droplet will then experience a force given by:

$$F_{jb} = \frac{d}{dy} \left( \frac{1}{2} C_d V^2 \right) = \frac{1}{2} \epsilon_0 \frac{\alpha}{y^2} V^2 \quad (1)$$

where  $C_d = \epsilon_0 \alpha / y$  is the droplet-to-charge electrode capacitance,  $\epsilon_0$  is the free space permittivity,  $V$  is the potential difference across the capacitor,  $\alpha$  is the effective plate area, and  $y$  is the distance between the lead and jet. This force is considered to act on a droplet with mass  $m$  for one droplet generation period,  $t_1$ , after which the velocity of the droplet in the direction of the force given by:

$$\vec{V}_{jb} = \frac{\vec{F}_{jb}}{m} t_1 \quad (2)$$

### Lead Deflection Force

The droplet, upon separation from the filament, retains a charge and will experience a force due to the field created by the potential on the charge electrode. The lead deflection field in JK was mapped out by an electrolytic tank experiment. At any point in the field, the charged droplet (considered a point charge) will be accelerated by the familiar electrostatic force:

$$\vec{F}_{ld} = q\vec{E}(y, z) \quad (3)$$

The total deflection of the droplet by this field is calculated by integrating this force over the trajectory of the droplet.

### Image Force

The third force considered in JK was the image force produced by the charged droplet in the proximity of the charge electrode and catcher. An image charge is pro-

---

Presented at *IS&T's 47th Annual Conference: The Physics and Chemistry of Imaging Systems*, May 15-20, 1994 in Rochester, New York.

duced by the electric field of the charged droplet modifying the surface charge density of any nearby conductors (or the polarization of dielectric objects). For example, placing a charged particle above an infinite conducting sheet rearranges the surface charge distribution in the sheet in such a way that the same electrostatic boundary conditions are produced as would obtain if the conducting sheet were replaced with a second, imaginary charged particle. This image charge has a polarity opposite that of the real charge and is found at a distance below the surface of the sheet equal to the distance of the real charge above the sheet<sup>2</sup>. In this model, the droplet is considered a point charge and the catcher surface an infinite conducting sheet.

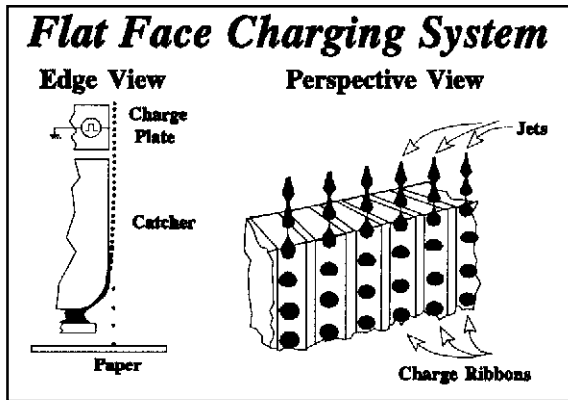


Figure 1. Unmodified Planar Charging Print Head

The magnitude of the image force on a charge  $q$  in front of an infinite conducting plane is:

$$F_{im} = \frac{kq^2}{(2y)^2} \quad (4)$$

where  $k=1/4\pi\epsilon_0$  and  $y$  is the distance from the charge to the sheet. The total deflection of the droplet by this force is found, as with the lead deflection force, by integrating the force over the trajectory of the droplet until it impacts the catcher surface, or escapes the print head.

### Discussion of JK Model

Inspection of the JK model shows that:

1) The lead deflection force requires an electrostatic field map, produced by an electrolytic tank model or finite element analysis of the print head configuration.

2) The image force is calculated considering a single droplet and its image. However, in an operating print head there are many droplets near the charge electrodes and catcher. Each droplet produces an electrostatic image that will interact with the real charges. Thus, the total image charge force on any one droplet will be the sum of the image charge forces produced by all droplets (superposition principle).

3) The droplet deflection for a single jet was calculated using the model, giving a  $2.41 \times 10^{-4}$  m deflection of the droplet at catcher impact from the undeflected trajectory. This compares with his experimentally measured value of  $2.29 \times 10^{-4}$  m. obtained with an unmodified print head.

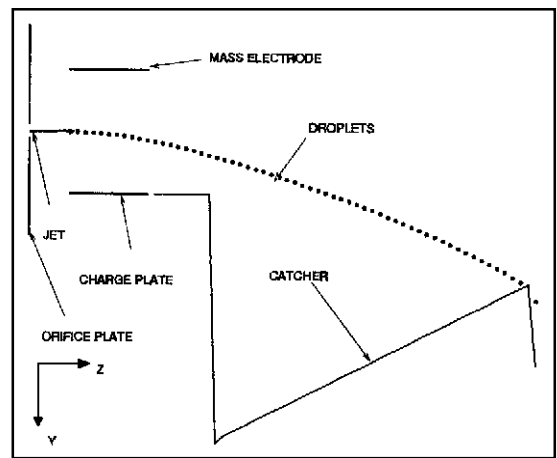


Figure 2. Print Head Configuration for Droplet Deflection Study

### Experiment with Modified Print Head

The modified print head shown in Figure 2 was used in a series of experiments designed to determine the effect of adding the mass charging electrode on droplet charging and deflection. A set of print head operating conditions (ink pressure, temperature, stimulation amplitude, etc.) were chosen and the voltages to the charging electrode (CEV) and mass electrode (MEV) were made the independent variables. The droplet charge and deflection at impact on the catcher face were the dependent variables, measured over a wide range of electrode voltages. The deflection of the droplets in the Y direction of Figure 2. from the undeflected trajectory is referred to as  $Y_d$ , while the distance from the top of the charge electrode to the impact point on the catcher (Z direction in Figure 2.) is referred to as  $Z_d$ . A typical set of data is given in Table 1.

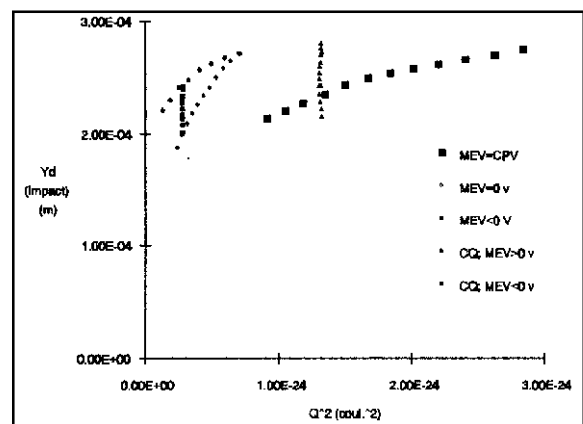


Figure 3. Impact Distance vs.  $Q^2$

Several sets of these data are plotted in Figure 3. as  $Y_d$  vs.  $Q^2$ . The series' labeled CQ are data where the droplet charge was held constant and appear as nearly vertical lines in the figure. This reveals one of the effects of adding the mass electrode: variable deflection of the droplets can be obtained without a corresponding change of the droplet charge. The series labeled MEV =

$0v$  is that which most nearly resembles the data that would have been obtained in an experiment using an unmodified print head.

### Analysis of Modified Print Head Data: JK Model

The data from the previous section were analyzed using the JK deflection model with two modifications: 1) the addition of the mass electrode allows an analytical expression for the deflection field in the charge electrode area, and 2) the image force calculation for droplet deflection was extended to include the contributions of 24 neighbor droplets.

#### Jet Bending Force

The droplet deflection due to jet bending was calculated using (1) and (2). A value for the parameter  $\alpha$  in (1) was determined from the droplet capacitance. The soundness of the parallel plate model for the droplet capacitance is displayed in Figure 4, a plot of the droplet capacitance,  $C_d$ , vs. the inverse of the jet-to-charge electrode spacing,  $1/y$ .  $C_d$  is found to be a very linear function of  $1/y$ , and  $\alpha$  can be calculated from the slope of the line in the figure.

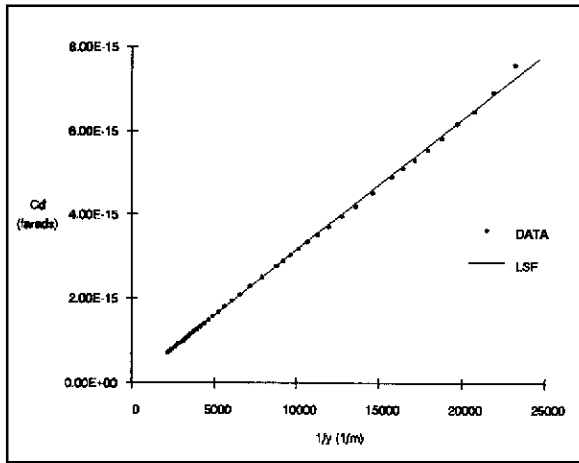


Figure 4. Droplet Capacitance vs.  $1/y$

#### Modified Lead Deflection Force

The magnitude of the deflection force on a droplet while passing through the charge and mass electrode region is calculated considering the droplet to be a point charge between two plates of a capacitor:

$$F_{ld} = -\frac{q(V_{ce} - V_{me})}{G} \quad (5)$$

where  $G$  is the distance between the charge and mass electrodes.  $V_{ce}$  and  $V_{me}$  are the charge and mass electrode voltages, respectively. Since the droplet is inductively charged by the electrodes, the sign of the induced droplet charge is the opposite polarity of the sum of voltages on the electrodes and is given by  $q = -C_d(V_{ce} + V_{me})$ . When  $F_{ld} > 0$  in (5), deflection is toward the catcher.

The lead deflection force acts on the droplets for a time,  $t_{ld}$ , determined by the charge/mass electrode length,  $L$ , and jet velocity,  $v_j$ , in the  $Z$  direction:  $t_{ld} = L/v_j$ . When integrated, (5) gives an expression for the magnitude of the droplet velocity in the  $Y$  direction,  $v_{ld}$ , as it leaves the charge/mass electrode region:

$$v_{ld} = \frac{C_d(V_{ce}^2 - V_{me}^2)t_{ld}}{mG} \quad (6)$$

where  $m$  is the droplet mass. As with  $F_{ld}$ ,  $v_{ld}$  is positive when the droplet is traveling toward the catcher.

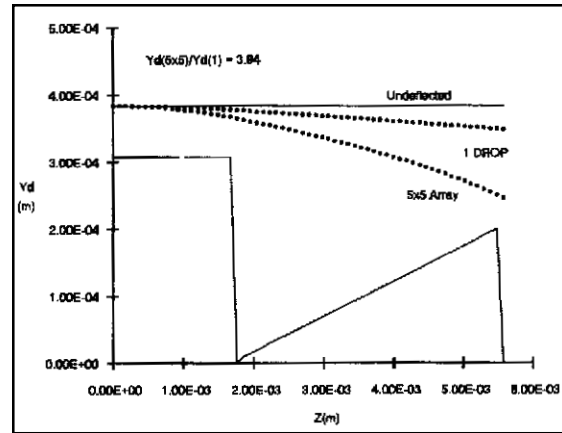


Figure 5. One and 5x5 Array Droplet Image Force Deflection

#### Modified Image Force

The effect of multiple image forces to droplet deflection is illustrated in Figure 5. The droplet trajectory was first calculated using a single, one droplet image force, given by (4). A second calculation was made using a 5x5 array of identical charges, separated from one-another by distances typically found in the modified print head. The total image force on the center droplet of the array is given by:

$$(F_{im})_0 = kq^2 \left[ \left( \frac{1}{R_0^2} \right) + \sum' \left[ \left( \frac{1}{R_{nm}^2} \right) \frac{R_0}{R_{nm}} \right] \right] \quad (7)$$

$R_0$  is the distance from the droplet array-center charge to its image charge,  $R_{nm} = [R_0^2 + (ma)^2 + (nb)^2]^{1/2}$  is the distance from the  $nm$ 'th charge in the image array to the droplet array-center charge,  $a$  and  $b$  are the array spacings, and  $\sum'$  indicates that the summation is over all  $n$  and  $m$  exclusive of the  $R_{00} = R_0$  term. This term is the center droplet self-image term and appears as the first term in parenthesis on the right-hand-side of (7).  $R_0/R_{nm}$  is the cosine of the angle between the force vector due to the  $nm$ 'th charge and the normal to the image plane.

Figure 5 shows that nearly a fourfold increase in deflection toward the catcher is realized with the  $5 \times 5$  array calculation over that of the single droplet calculation. The total force due to array images continues to grow as the array becomes larger<sup>3</sup>. The  $5 \times 5$  array was chosen to include the most important contributions with-

out generating a significant error from the assumption made in (7) - that all droplet charges in the summation are equidistant from the image plane.

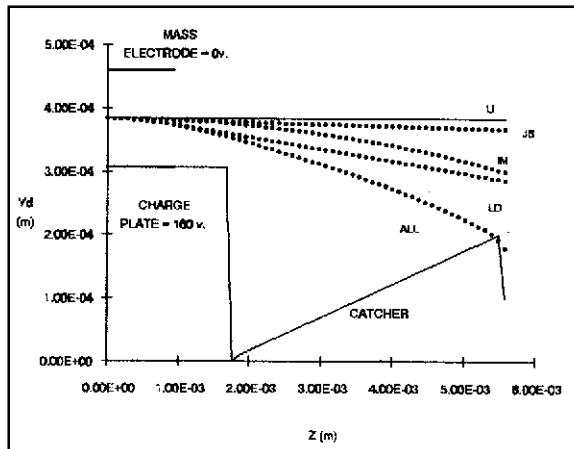


Figure 6. Deflection Mechanisms from JK

## Results

The contributions to the droplet deflection from jet bending, lead deflection, and image forces are shown for a set of standard print head conditions and voltages in Figure 6. The trajectory a droplet would have for the jet bending force alone is shown as curve JB. Likewise, for the lead deflection and image forces only, the trajectories are labeled LD and IM. The curve labeled ALL shows the droplet deflection for all of the mechanisms acting in concert. Table 2 contains the percentage of the total deflection each mechanism makes from these calculations from the modified JK model, along with those from JK.

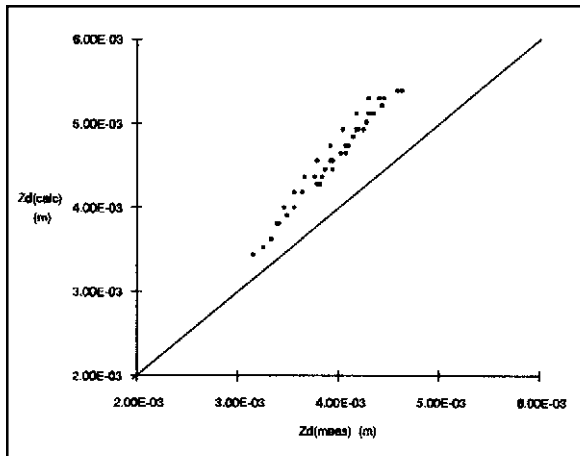


Figure 7. JK Predicted vs. measured droplet deflection

The distance from the top of the charge electrodes to the point where the droplets impact the catcher surface,  $Z_d$ , was calculated using the JK model with the measured values of CEV and MEV as input parameters. The values for  $Z_d(\text{calc})$  are compared to the experimentally measured values,  $Z_d(\text{meas})$ , in Figure 7. The diagonal line in this correlation plot is  $Z_d(\text{calc})=Z_d(\text{meas})$ .

All of the points fall above and at a slight angle to this line, showing that the predicted values for  $Z_d$  are consistently larger than those for the measured values. The larger values of  $Z_d(\text{calc})$  are due to smaller calculated droplet deflections. This results in the calculation droplet traveling farther in the Z direction than the measured droplet before impacting the catcher.

## Infinite Sheet of Charge Model

### Introduction

Two concerns of the modified JK model were noted while analyzing the experimental data acquired with the modified print head:

1) The lead deflection force is “turned off” immediately after the droplet leaves the region between the charge and mass electrodes. This ignores the fringing fields that exist beyond the edges of these electrodes.

2) The image force on a droplet in motion in front of the catcher/charge electrode is difficult to calculate accurately. The difficulties include the nonplanar, finite geometry of the catcher; the bookkeeping required to track each droplet in the array individually for a proper summation in (7); and the finite drop size. For a droplet at a distance comparable to the droplet diameter from the catcher surface, a separate calculation may be necessary to determine the charge distribution for each droplet (an infinite series of charges inside the droplet volume<sup>4</sup>) resulting in the effective location of the droplet charge no longer coinciding with the center of the droplet.

Another model was developed to simplify the image force calculation and handle the fringing field problem in a way that does not require an outside experiment or extensive finite element calculations. It is semi-empirical in nature and contains two adjustable parameters—one for the lead deflection calculation and another for the image force. The jet bending force from JK was considered adequate and is used in its unaltered form.

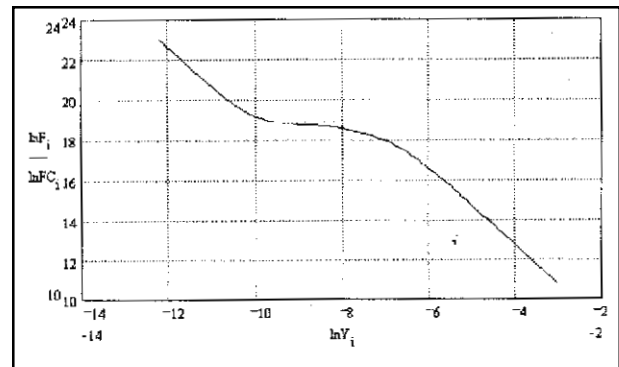


Figure 8. log-log plot of  $F_i/q^2$  vs. distance for 20x20 array

### Image Force

In order to simplify the image force calculation, a single value for this force is calculated and used in place of (7). An initial value for this force is obtained from an image force calculation for the center charge of an array of charges as a function of distance from the image plane. Figure 8. shows a plot of the reduced force,  $F_i = F/kq^2$

(solid line), from a calculation made for a  $20 \times 20$  point charge array.

The force exhibits three distinct ranges of behavior:

1) single droplet image force behavior where the force varies as  $1/Y^2$  from the extreme left-hand-side to about  $\ln Y_i = -10$  (45 microns),

2) infinite sheet of charge behavior from  $\ln Y_i = -10$  to  $\ln Y_i = -8$  (335 microns), where the force is nearly independent of distance, and

3) lumped particle behavior from  $\ln Y_i = -6$  (2.5 mm) to the extreme right-hand-side, where the force is again  $\sim 1/Y^2$ , but with the effective image charge equal to the total charge of the array, instead of a single charge (i.e., the distance is becoming large enough that the array begins to take on the appearance of a point charge).

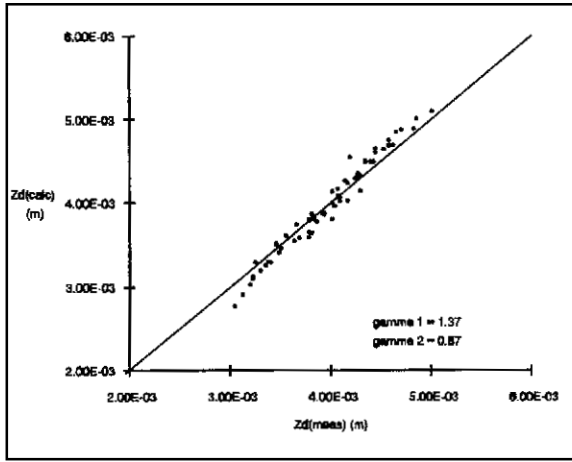


Figure 9. Infinite sheet of charge droplet deflection plot

The radius of the ink droplets used in the modified print head experiment is 42 microns and the average distance from the undeflected droplets to the catcher face is 219 microns. These dimensions fall in the range of the infinite sheet behavior region and suggest a reasonable initial value for the approximation for the image force over the entire droplet trajectory. The magnitude of the force on a charge  $q$  in front of an infinite sheet of charge having a surface charge density  $\sigma = q/ab$  is given by:

$$F_{isc} = q \frac{\sigma}{2 \epsilon_0} = \frac{q^2}{2 \epsilon_0 ab} \quad (8)$$

where  $a$  and  $b$  are the charge spacings in the array. The dotted line in Figure 8 is the value for the reduced force  $FC_i = F_{isc}/kq^2$  for a charge in the field of an infinite sheet of charge, and follows the solid curve very closely for  $Y_i$  between  $-10$  and  $-8$ . In addition, the average value of  $F_i/kq^2$  for  $Y_i$  in this range is  $1.66 \times 10^8 \text{ m}^{-2}$ , which compares well with the value of  $FC_i = 1.56 \times 10^8 \text{ m}^{-2}$ , calculated using (8).

## Results

The use of a single valued image force for the droplets over that portion of the trajectory greatly simpli-

fies the calculation of the droplet impact point on the catcher face. Once the velocities  $v_{jb}$  and  $v_{ld}$  have been calculated, the equation for the position of the droplet in the  $Y$  direction is given by the constant acceleration equation:

$$Y_d = Y_{d0} + V_{jb}t_f + \gamma_1(V_{ld}t_f) + \gamma_2 \left( \frac{q^2}{4mab \epsilon_0} \right) t_f^2 \quad (9)$$

where  $m$  is the droplet mass,  $t_f$  is the time of flight of the droplet,  $Y_{d0}$  is the initial position of the droplet,  $v_{jb}$  is from (2),  $v_{ld}$  is from (6), and  $\gamma_1$  and  $\gamma_2$  are the adjustable parameters, which will be discussed later.

The unknown,  $t_f$ , is determined by noting that the position of the catcher face,  $Y_c$ , is a function of  $Z$  and is catcher geometry dependent. The position of the droplet in the  $Z$  direction is  $Z_d = v_j t_f$ , where  $v_j$  is the jet velocity in the  $Z$  direction. The value for  $t_f$  at droplet impact on the catcher face,  $t_{fi}$ , is obtained by setting  $Y_c = Y_d$ . Once  $t_{fi}$  has been determined, the position of the droplet impact is known.

The adjustable parameter,  $\gamma_1$ , in (9) is used to account for the fringing field at the edges of the mass and charge electrodes. Using a value for  $\gamma_1 > 1$ , is equivalent to using a longer *effective* lead length for calculating the amount of lead deflection.  $\gamma_2$  is an adjustable parameter to fine tune the strength of the (constant) image force and act as a correction factor for the approximations that were made.

Table 1. Typical droplet charge and deflection date.

Charge Electrode Voltage (volts)	Mass Electrode Voltage (volts)	Droplet Charge (pC)	Yd Droplet Deflection (mm)
170	0	0.56	0.209
180	-20	0.53	0.213
160	30	0.63	0.213
130	210	1.15	0.216
150	150	1.02	0.221
250	-100	0.50	0.241
250	90	1.15	0.281

Table 2. % Total deflection for each mechanism & model.

	JB	LD	IM
JK[Ref. 1]	9.5	49.5	41.0
Modified JK	8.1	49.2	42.6
ISC	10.2	45.4	44.4

The model is calibrated with experimental data by simultaneously varying  $\gamma_1$  and  $\gamma_2$  to minimize the sum of the squares of the difference:  $\Delta Y = Y_d(\text{meas}) - Y_d(\text{calc})$ . The same modified print head data used with the JK model was analyzed using this model and the values for  $Z_d$  at impact were calculated. These calculations yielded the best fit with values of  $\gamma_1 = 1.37$  and  $\gamma_2 = 0.87$ . The

correlation plot of  $Z_d(\text{calc})$  vs.  $Z_d(\text{meas})$  for this model—similar to Figure 7 for the JK model—is shown in Figure 9. The diagonal line in Figure 9 is the  $Z_d(\text{calc}) = Z_d(\text{meas})$  line and, as can be seen, the calculated and measured data are in good agreement.

It is not too surprising that the calculated data from this model is in better agreement with the experimental data than that generated by the JK model, since there are two adjustable parameters. One the other hand, if the model were unreliable, minimizing the measured and calculated difference  $\Delta Y^2$  would not necessarily produce good agreement. Table 2 shows the relative percentages for the three deflection mechanisms for the infinite sheet of charge model (ISC) along with the previously presented results from JK. The contributions from each mechanism have similar values in all three models, indicating that the replacement of the image force calculation (7) with a constant value did not produce a radically different result.

### Summary

A binary continuous ink jet print head was modified by the addition of a mass charging electrode opposite the

jets and parallel to the standard charging electrodes. Data for droplet charging and deflection were recorded for a variety of electrode voltages.

These data were analyzed using a modified version of an existing droplet deflection model (JK) and a recently developed model. The new model is semi-empirical, having two adjustable parameters, and is based on: 1) the charged droplet image forces resembling those from an infinite sheet of charge, and 2) the lead deflection force fringing fields. Once the parameters have been determined by a sample set of data, this model greatly decreases the computational complexity and improves the accuracy for predicting the droplet impact point on the catcher face.

### References

1. J. A. Katerberg, Drop charging and deflection using a planar charge plate, *The Fourth International Congress on Advances in Non-Impact Printing Technologies*, New Orleans, **March 1988**, pp. 241-249.
2. E. M. Pugh and E. W. Pugh, *Principles of Electricity and Magnetism*, Addison-Wesley, NY, 1970, pp. 89-90
3. R. Fagerquist, *Kodak Memo*, January 1990, unpublished.
4. Pugh, *op. cit.*, pp. 91-92.